地理学論集
Vol. 92, No. 1（2017）

Geographical Studies
Vol. 92, No. 1（2017）

Analysis of the Strong Local Wind in Northwestern Hokkaido, Japan

Koki KASAI[1], Keiji KIMURA[2], Kei SHIOMI[3,4], Atsushi KONNO[4], Takeo TADONO[3,4] and Masahiro HORI[3,4]

Abstract

A strong local wind has been observed in Rumoi, northwestern Hokkaido, Japan. In order to investigate the wind around Rumoi, an analysis was performed using 30-year AMeDAS wind observations and numerical experiments with the Weather Research and Forecasting (WRF) model. Observation results show that there is a frequent strong wind in Rumoi in comparison with other areas around Rumoi. In relation to seasonal changes in wind direction, more than 50% of the wind in summer blows from ESE, but westerly winds are frequent in winter. To clarify the mechanisms involved in producing a strong local wind in winter, we compared two events using observations and numerical experiments. One case involves a strong local wind with a speed of approximately 12 m/s in Rumoi and a weak wind of less than 5 m/s in the surrounding areas; the prevailing wind direction is ESE (03:00 on January 28, 2003). The other case is that of a strong wind over 10 m/s blowing over the entire study area (on the afternoon of March 8, 2005), with a westerly prevailing wind. The experimental results show a relatively good correspondence with those of the observation. A cross-section view demonstrates the existence of a mountain wave when the strong local wind is observed in Rumoi. The wind then passes through the valley-shaped topography, and wind speeds are accelerated in the vicinity of Rumoi, which suggests the existence of a gap wind. Additionally, a sensitivity experiment is performed by changing the land surface model without considering snow, and the wind speed over land is seen to be reduced by 2 m/s, with very little change in the wind direction.

Key words: local wind, numerical experiment, statistical analysis, wind speed, influence of topography

I. Introduction

Wind consists of the bulk movement of air. In the fields of mesoclimatology and microclimatology, it is necessary to gain an understanding of the distribution of meso-β scale winds to explain the distribution of temperature and precipitation (Kawamura, 1963). In a study conducted over a large area in Japan, Kawamura (1966, 1981) investigated the distribution of winds over central Japan and the Kanto Plain. In the above-mentioned previous studies, the surface wind distribution was estimated by the prevailing wind direction, and determined according to wind roses of the most frequent wind direction. Suzuki (1991, 1992) used ground-based observation data and focused on the wind over central Japan to clarify the response of surface wind speed and direction to the synoptic pressure gradient. In these studies, it is acknowledged that the observed wind includes both the effect of synoptic pressure gradient and that of local circulation.

The present study focuses on an analysis of wind speed and wind direction in the area of Rumoi, Hokkaido, Japan (Fig. 1). Japan lies predominantly within the temperate climate zone, but the Hokkaido and Tohoku regions lie on the main transition band between temperate and subarctic climates (Kasai and Kimura, 2013). Therefore, Hokkaido experiences a subarctic climate, and most of the region is covered with snow in winter. Kawamura (1963) investigated the surface wind distribution in Hokkaido, and classified eight types of large-scale flow patterns during winter. Winds in the area of Rumoi blow from W or ESE direction. Kato (1983) analyzed daily mean wind speed and surface pressure data using a principal component analysis to investigate the wind distribution in Hokkaido. The author suggested that W and ESE winds blew over Rumoi as the primary and third principal component, respectively. Suzuki (1994) also analyzed the surface wind over the coastal area surrounding Japan (including Rumoi); the direction

[1] Graduate student, Graduate School of Information Science and Technology, Hokkaido University, Sapporo, Japan

[2] Faculty of Letters, Nara University, Nara, Japan

[3] Earth Observation Research Center, Japan Aerospace Exploration Agency, Tsukuba, Japan

[4] Graduate School of Information Science and Technology, Hokkaido University, Sapporo, Japan

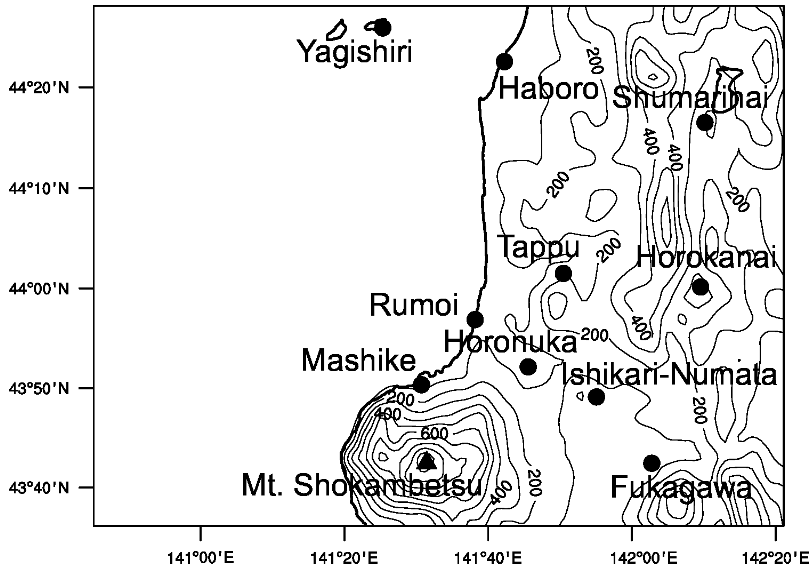

Fig. 1. Study area
Circles indicate AMeDAS locations around Rumoi. A triangular denotes the summit of Mt. Shokambetsu.

of the land (sea) breeze was shown to be ESE (WNW). However, these previous studies focused on the entire area of Hokkaido or on ground observation points in the coastal area, and therefore, the distribution of the local wind in the northwestern part of Hokkaido has not yet been adequately clarified. Currently, we can analyze this in detail using the meteorological dataset of long-term multipoint observations to investigate not only the mean field, but also local events such as strong winds.

Winds that are influenced by local topography and restricted to a range of 100 km or less are known as local winds (Defant, 1951). In studies of local winds in Hokkaido, Kawai et al. (2008) researched the climatological characteristics of the local wind in Tokachi district. In addition, Sagawa (2004) carried out field observations and analyzed the strong wind blowing in the Suttsu region in the western part of Hokkaido, concluding that both the area of strong wind and the discontinuity line of the wind speed in Suttsu were related to the valley-shaped area. These previous studies discussed local winds using observational data and/or reanalysis data, and therefore, spatial wind distributions were not clarified. Furthermore, there are no existing studies to date analyzing wind distribution in the northwestern part of Hokkaido using meteorological models.

Numerical simulations are performed to determine the strong local wind and its spatial distribution in the area of Rumoi. In order to adequately study the local wind, abundant meteorological data are required. However, there is only a small volume of obtainable observed data at a certain spatial resolution, and therefore it is necessary to perform additional numerical simulations to determine the spatial distribution of a number of meteorological factors. For example, Prtenjak et al. (2010) investigated the interaction of a summer frontal bora and the sea-land breeze along the northeastern Adriatic coast, and Belušić et al. (2013) also studied the Adriatic bora wind using a numerical model simulation. In addition, Powers (2007) simulated the major Antarctic event of the May 2004 McMurdo windstorm, and Steinhoff et al. (2013) analyzed a case study of a representative summer foehn event in order to identify and explain the McMurdo Dry Valleys foehn mechanism. In Japan, Kawaguchi et al. (2010) analyzed Yamase, which is a cold, humid, northeasterly wind blowing towards the coast on the Pacific side of the Tohoku region during summer, which blows in a southerly direction in the Kitakami Basin. Furthermore, Sasaki et al. (2010) performed numerical simulations of the strong southeasterly “Kiyokawa-dashi” wind in Yamagata, Japan, during the summer, and reproduced it at a resolution of 1 km. Inamura et al. (2009) carried out a numerical experiment to investigate a local wind known as the Matsubori-kaze, and discussed the influence of the unique topography of Mt. Aso, Kumamoto. Similarly, Sakamoto et al. (2014) investigated the simulation and mechanism of the Matsubori-kaze.

Weather simulation models are not exclusively used for investigations of wind speed and direction, and are also used to model other meteorological factors. Takane et al. (2013) investigated the actual conditions of mesoscale summer high temperatures recorded in the Osaka-Kyoto urban area of Japan using a numerical simulation as well as an observation network and found that a significant amount of heat was transported from the tropics at the synoptic scale and/or mesoscale and airflow also contributed to the high temperature events.

When using meteorological models, it is useful to make sensitivity studies of model parameters to evaluate and understand the model accuracy and characteristics. Previous studies have investigated meteorological model sensitivity using different dataset input methods (Tatsumi et al., 2008; Akimoto and Kusaka, 2010; Zhang et al., 2012). In addition, numerical simulations have been applied over complex terrain in order to evaluate the ability of meteorological models (Jiménez and Dudhia, 2013; Zhang et al., 2013). Horvath et al. (2012) performed sub-kilometer dynamical downscaling using the Weather Research and Forecasting (WRF) (Skamarock et al., 2008) and Mesoscale Model Version 5 (MM5) models (Grell et al., 1994), and considered the characteristics of these models. In the present study, as the study area is covered with snow during the winter season, a sensitivity experiment is performed to evaluate the influence of the land's surface.

The present study has three main aims, as follows. Firstly, this study applies a statistical analysis of the wind speed and direction to the area of northwestern Hokkaido (around Rumoi). Secondly, the strong local wind in Rumoi is modeled using numerical experiments, with the aim of reproducing the observed weather conditions during data collection and to show the spatial distribution of the wind. In addition, the experimental result is then compared with a strong wind event that occurred over the entire area of Rumoi. Finally, the influence of the topography around Rumoi is discussed as being the mechanism for the strong local wind, and a sensitivity experiment is conducted to understand the change in winds in relation to a change in land surface schemes, with or without the consideration of snow.

A statistical analysis of the wind around Rumoi is described in Chapter 2, and the methodology used to select the strong local wind event in the area is explained. The model datasets used in this study are explained and a summary of the WRF model is provided in Chapter 3. Two types of meteorological data are used, sea surface temperature (SST) and digital elevation model (DEM) data, and the numerical method used in this study is described, together with the nested domains. The two reproductive experimental results of the WRF are shown in Chapter 4. Chapter 5 discusses the orographic wind, which is the source of the strong local wind in Rumoi, and the result of a sensitivity experiment is also shown. Finally, Chapter 6 provides a summary of this study.

II. Local wind around Rumoi

1. Statistical wind analysis

A statistical analysis was performed to gain an understanding of the wind movement around Rumoi, and the observation datasets of the Automated Meteorological Data Acquisition System (AMeDAS) operated by the Japan Meteorological Agency (JMA) were used for this analysis. The observation points were Rumoi, Mashike, Haboro, Horonuka, Ishikari-Numata, Fukagawa, Tappu, Shumarinai, Horokanai, and Yagishiri (see Fig. 1) and the meteorological elements were the daily mean wind speed, daily maximum wind speed, and the most frequent daily wind direction. Data from the period 1981 to 2010 were used as normal values, but from Haboro the daily mean wind speed data were available only from 1981 to 1999, and the daily maximum wind speed from 1981 to 2002, due to discontinuous datasets.

Figure 2 shows the mean and maximum wind speeds recorded at the observation points. The mean wind

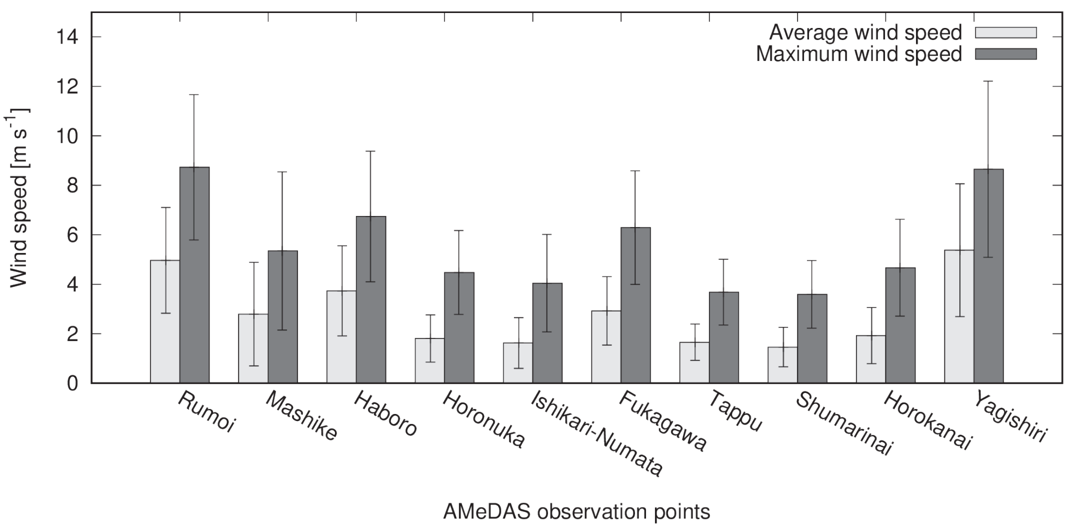

Fig. 2. Wind speed comparison
White and gray bars indicate average wind speed and maximum wind speed of the AMeDAS observation points, respectively. Error bars represent standard deviations.

speed in Rumoi was approximately 5.0 m/s, which is the second highest recorded speed. The highest wind speed was recorded in Yagishiri (approximately 5.4 m/s) on a remote island of Hokkaido, and hence, the wind speed in Rumoi is relatively strong compared to other locations in northwestern Hokkaido. The mean wind speed at coastal locations (Rumoi, Mashike, and Haboro) was higher than those in other areas. However, the speed recorded at Fukagawa was an exception, as it was strong in spite of being an inland location. The lowest wind speed was recorded at Shumarinai (approximately 1.5 m/s), and the mean wind speed of the observation points located inland (except Fukagawa), and consisting of Horonuka, Ishikari-Numata, Tappu, Shumarinai, and Horokanai, was less than 2 m/s. The maximum wind speed had the same tendency as that of the mean wind speed, although the maximum wind speed of Rumoi (approximately 8.7 m/s) was slightly higher than that of Yagishiri. The lowest maximum wind speed was recorded at Shumarinai, at approximately 3.6 m/s.

A wind frequency analysis was then conducted to understand the frequency of the strong winds recorded at the observation points. The winds speeds were divided into intervals of 5 m/s up until the daily maximum wind speed, and Fig. 3 shows the result of the frequency distribution, where it is evident that Rumoi had the least frequency (7%) of weak winds (< 5 m/s). The weak wind (< 5 m/s) occupied more than half of the wind in Horonuka, Ishikari-Numata, Tappu, Shumarinai, and Horokanai. Rumoi recorded the second largest number of days with a maximum wind speed of more than 10 m/s, after Yagishiri. This shows that the wind in Rumoi was strong in both frequency and wind speed. In addition, there were minor frequencies of strong winds (> 20 m/s) in Rumoi (0.11%), Fukagawa (0.06%), and Yagishiri (0.68%).

As the above results related only to wind speed, an analysis was also performed in relation to wind direction. Wind roses were made on the basis of the daily most frequent wind direction at the observation points. Figure 4 shows the wind roses for an entire year, and during winter (DJFM) and summer (JJAS). From an analysis of the annual wind roses, it is evident that Rumoi, Horonuka, Fukagawa, Tappu, Shumarinai, and Horokanai experience two main wind directions with no seasonal changes occurring in these wind directions, even when the frequency of the wind changes. These winds are, therefore, considered to be the prevailing winds at each location. Mashike and Haboro also experience two dominant wind directions, but seasonal change exists in the wind direction frequency. Ishikari-Numata has three most frequent wind directions (NE, S, and NW). In addition, the wind roses of Yagishiri show various directions, and it is therefore evident that no prevailing wind direction exists at Yagishiri.

In relation to seasonal change, more than 50% of the wind blows from ESE in Rumoi during summer. In winter, however, the westerly wind is more frequent (at more than 30%), although the ESE wind continues to blow in Rumoi. In a previous study, Kato (1983) divided the observation points into four kinds of wind systems to clarify regional characteristics of the wind in Hokkaido, and Rumoi was then classified into clusters where the wind from the west changes seasonally. During winter in Mashike, Haboro, Tappu, Shumarinai, and Yagishiri the wind tends to blow from northward in contrast to summer, but the wind roses of Fukagawa and Horokanai rarely change seasonally.

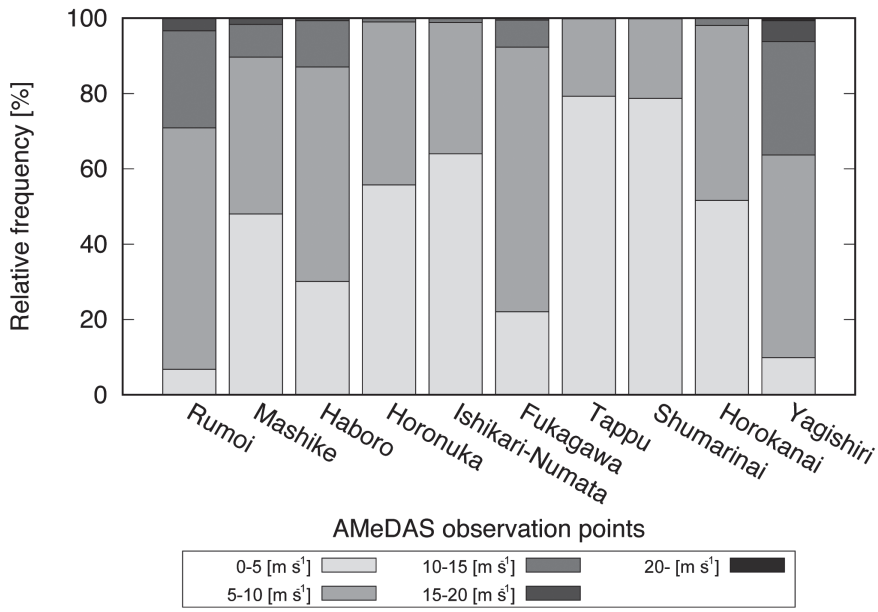

Fig. 3. Frequency distribution of maximum wind speed between the AMeDAS observation points

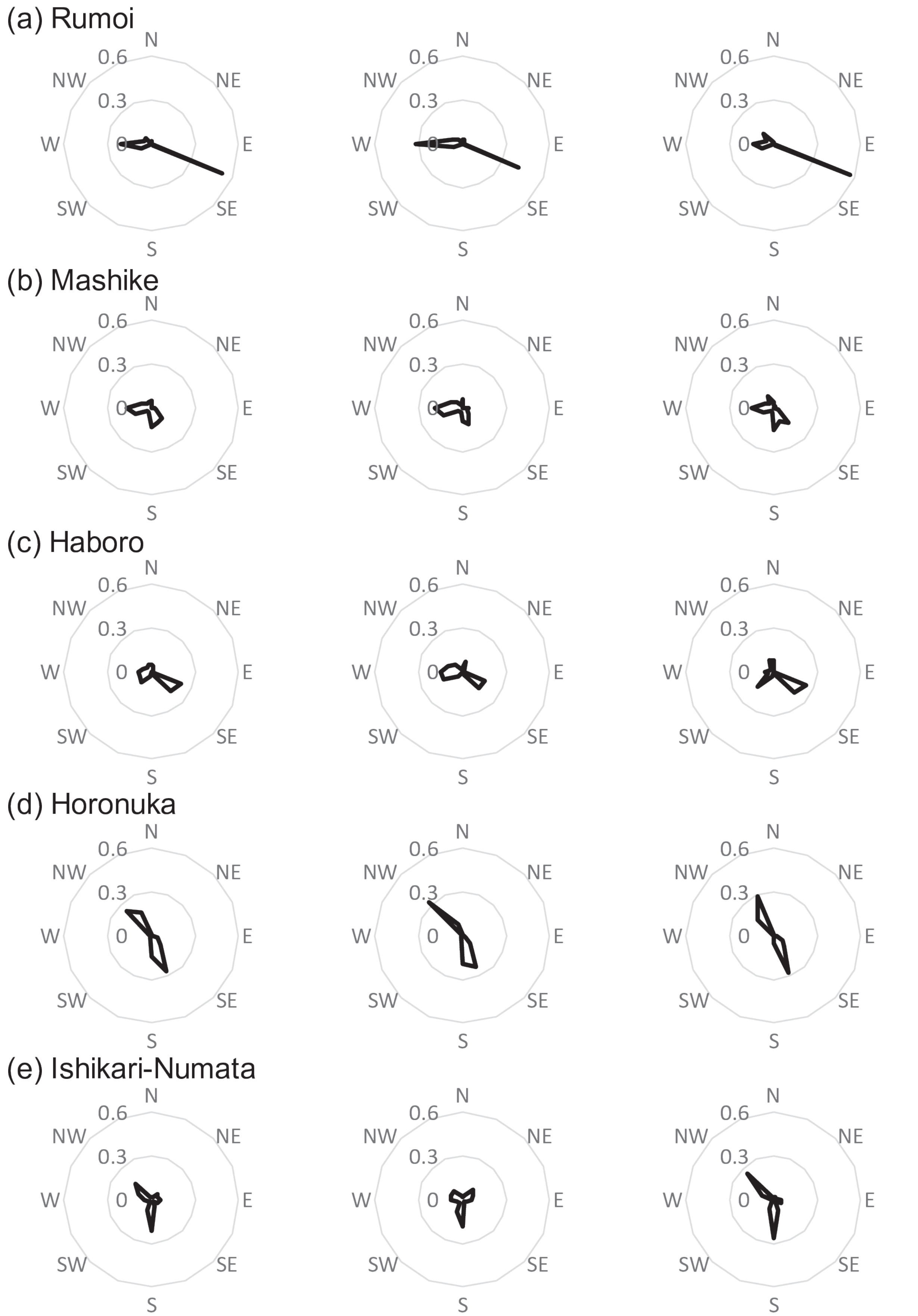

Fig. 4. Wind roses for the AMeDAS observation points (a–e)
Three wind roses for each observation point, representing (from left to right) annual, winter (DJFM), and summer (JJAS) prevailing winds, respectively.

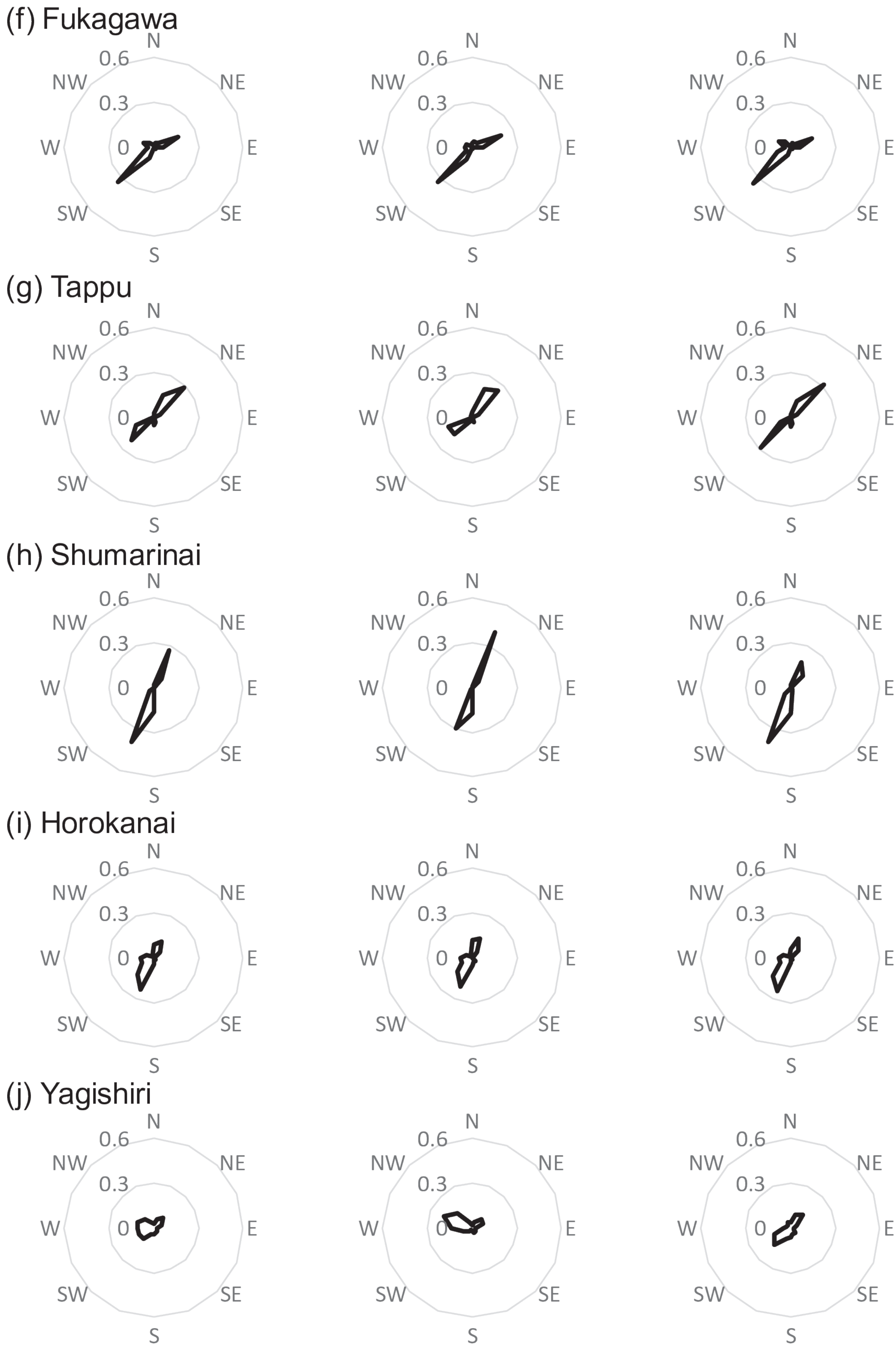

Fig. 4. Continued (f–j)

2. Selection of events

This subsection describes the methodology used to select strong local wind events around Rumoi. As shown in Fig. 2 and Fig. 3, Rumoi has a wind speed higher than the surrounding AMeDAS observation points, and strong winds blow frequently (except for Yagishiri, which is located on a remote island). It is evident from results of analysis of the most frequent wind direction in Rumoi (Fig. 4a), that the two main wind directions are ESE and W.

This study uses numerical experiments with the WRF model to clarify the condition of the wind on a day when a strong local wind occurred in Rumoi. To achieve this aim, the strong wind record observed in Rumoi is investigated. For comparative purposes, data for Mashike and Haboro were also checked, as these are coastal areas proximal to Rumoi (Fig. 1). Here, a correlation analysis is performed between Rumoi and Mashike, and between Rumoi and Haboro using wind speeds recorded every 1-hr. Table 1 shows the result of the correlation analysis focusing on the two main wind directions in Rumoi. When the prevailing wind direction is ESE, the correlation coefficient has a lower value of less than 0.3, and a regression coefficient of 0.07–0.22. Using a comparison of the regression coefficients, it is evident that Rumoi experiences an ESE wind that is over four times stronger than at the other locations. However, when the W wind prevails in Rumoi, the wind speed in Rumoi correlates strongly with that in surrounding areas (correlation coefficient ~0.8), and the regression coefficient is larger compared to the case of the ESE wind.

A strong wind event occurring in Rumoi at 03:00 LST on January 28, 2003, was selected for the first case, as it occurred concurrently with a weak wind event in Mashike and Haboro. The wind direction in Rumoi at this time was ESE (shown in Fig. 10 compared with numerical experiments). The wind speeds in Rumoi, Mashike, and Haboro were 11.9 m/s, 3 m/s, and 2.2 m/s, respectively. The pressure pattern at this time was obtained from objective analysis datasets and is shown in Fig. 5. Figure 5a shows low pressure located over the Sea of Japan to the west of Hokkaido at 03:00 LST January 28, 2003, which is consistent with the wind direction in Rumoi. In addition, as a contrasting second case, 15:00 LST March 8, 2005, was selected because western winds dominated in Rumoi, Mashike, and Haboro (shown in Fig. 14). The wind speed at the three points was similar (from 11 m/s to 15 m/s) and this is therefore an example of a non-locally strong wind occurring in relation to Rumoi. From the pressure pattern at this time (shown in Fig. 5b), the pressure gradient is in a north-south direction in Hokkaido. By setting events based on the two main wind directions occurring in Rumoi, this study then aims to clarify the different characteristics of the wind conditions in this study area via numerical experiments.

III. Experimental design

1. Initial data

National Centers for Environmental Prediction (NCEP) Final (FNL) Operational Model Global Tropospheric Analyses product (NCEP/National Weather Service/NOAA/U.S. Department of Commerce, 2000) is used as input meteorological data, as it has spatial ranges covering all over the world. The datasets were prepared every 6 h on 1° × 1° grids. The analyses are available on the surface and at 26 levels from 1000 hPa to 10 hPa. In addition, meso-objective analysis (MANAL) datasets by JMA were also used in the experiment, because their spatial resolution is 10 km, which is finer than that of the FNL. The temporal resolution of MANAL is the same as that of FNL (six-hourly). MANAL datasets consist of U and V components for wind, temperature, relative humidity, pressure reduced to mean sea level, and geopotential height. MANAL was selected as the main product for use, although FNL was used for supplementary elements that were not recorded in MANAL.

The SST data used were the Optimum Interpolation Sea Surface Temperature (OISST) by NOAA (Reynolds et al., 2007), which were prepared separately using the meteorological datasets. OISST has a spatial resolution of 1° × 1°, which is equivalent to that of the FNL. However, it has a temporal resolution of one week (168 h), because SST changes minimally in time compared to other meteorological variables.

The DEM datasets used in the present study were provided by the Geospatial Information Authority of Japan, and cover an area of Japan from 40°N north, excluding Etorofu, Kunashiri, Shikotan, and Habomai islands, with a spatial resolution of 10 m, which is much finer than the original DEM datasets of the WRF model.

Table 1. Statistics from correlation analysis of observed wind speed in 2003 and 2005

	Wind direction	Rumoi vs. Mashike		Rumoi vs. Haboro	
		2003	2005	2003	2005
Correlation coefficient	ESE	0.09	0.11	0.25	0.28
	W	0.81	0.89	0.85	0.78
Regression coefficient	ESE	0.07	0.11	0.19	0.22
	W	1.00	1.02	0.69	0.64

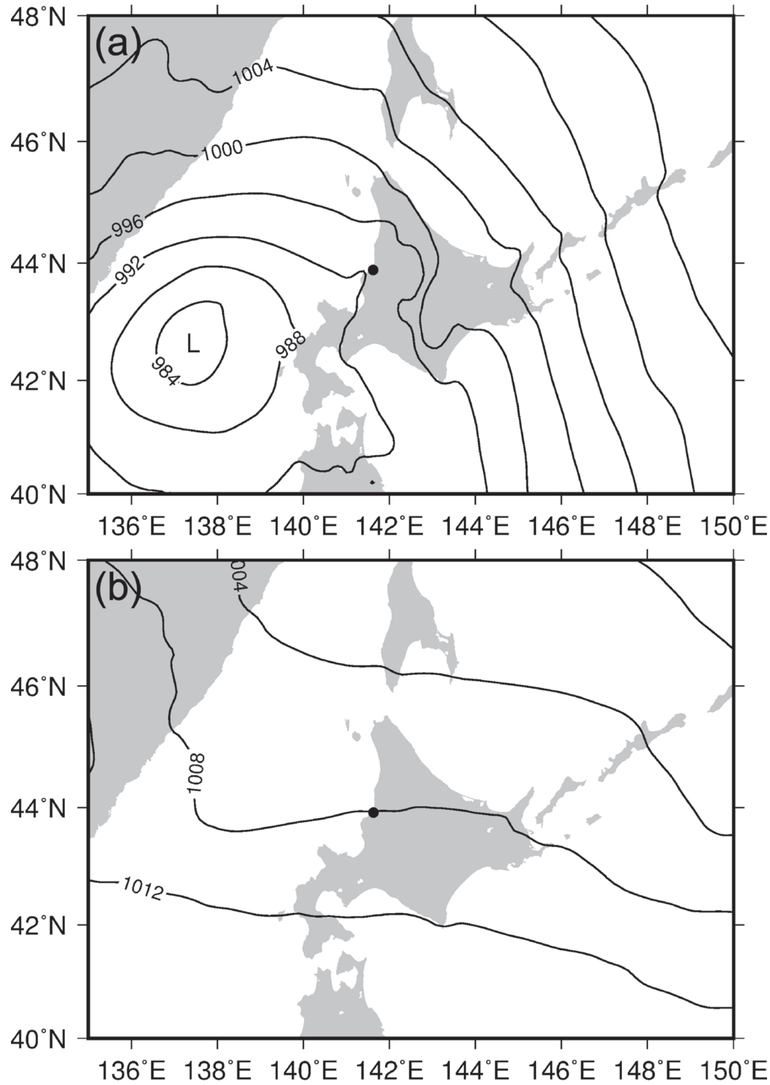

Fig. 5. Pressure distribution chart (a) at 03:00 LST on January 28, 2003 and (b) 15:00 LST March 8, 2005 by using MANAL datasets
The contour lines represent the isobaric lines of 4 hPa, and the black circles indicate the location of Rumoi. The description of MANAL datasets is shown in section 3.1 because the datasets are used as input data for numerical experiments.

2. Meteorological model and experimental domains

Meteorological models, particularly mesoscale meteorological models, are widely used as analysis tools in engineering and agriculture, as well as in meteorology (e.g., Kusaka, 2009). The WRF model is a numerical weather prediction and atmospheric simulation system designed for both research and operational applications. The WRF effort is the result of a collaboration between university scientists at the National Center for Atmospheric Research's (NCAR) Mesoscale and Microscale Meteorology Division, NOAA's NCEP and Earth System Research Laboratory (ESRL), the Department of Defense's Air Force Weather Agency (AFWA) and Naval Research Laboratory (NRL), the Center for Analysis and Prediction of Storms (CAPS) at the University of Oklahoma, and the Federal Aviation Administration (FAA) (Skamarock et al., 2008). WRF version 3.6.1 was released on August 14, 2014, and is used in this study.

The experimental timeframes used were from 21:00 LST on January 27, 2003 to 09:00 LST on January 28, 2003; and from 09:00 to 21:00 LST on March 8, 2005. In the two numerical experiments, the settings used are identical: 6-hr prior to and after the event time. The spin-up period is estimated as 6–12 hr with a spatial resolution of 10 km (Skamarock, 2004), and 4–6 hr with that of 4 km (Weiss, 2008). These periods are shorter than those used in previous studies because of the spatial resolution of 1 km in the innermost domain.

When downscaling was applied in this experiment, the two-way nesting method was used, and Fig. 6 shows the three nested experimental domains. The center point of the outermost domain is located at 44°N and 141.5°E. The outermost domain has a grid spacing of 9 km (132 × 120 grids), and this was decreased by a factor of three for each of the nested domains; hence, the spatial resolution of the innermost domain is 1 km (208 × 208 grids). The DEM

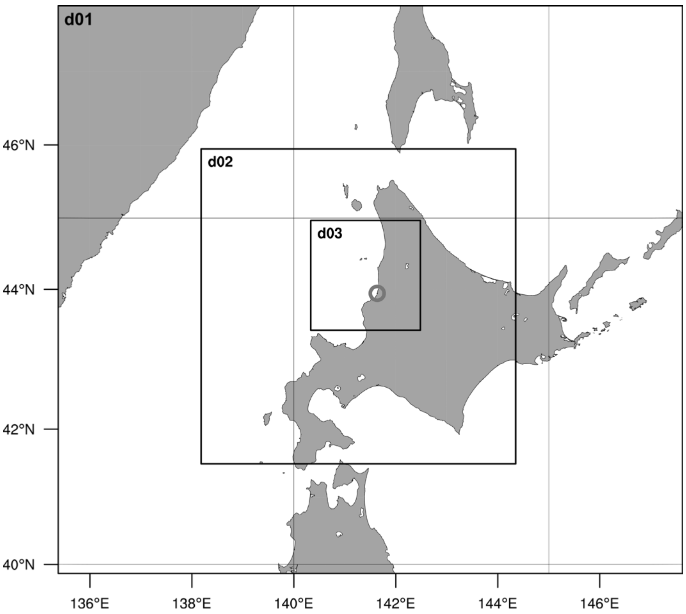

Fig. 6. Experimental domains used in this study
The largest domain (d01) is represented by the outline of the figure; a circle indicates the location of Rumoi.

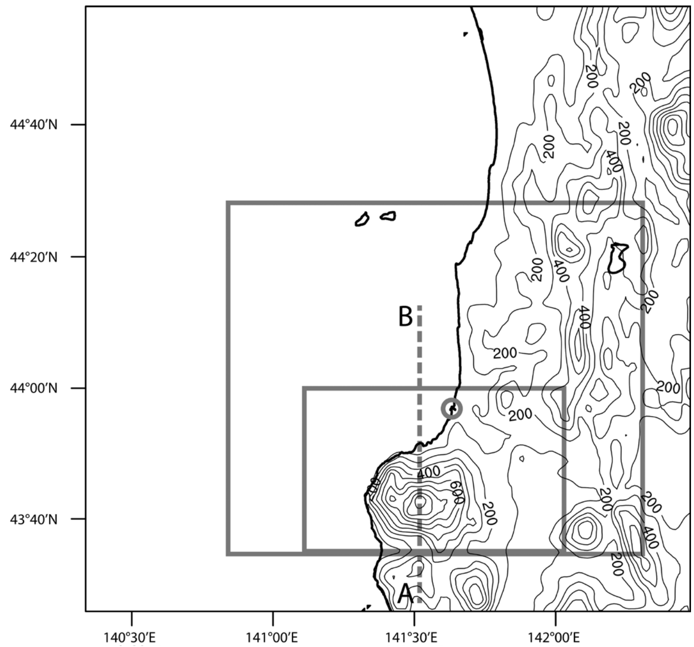

Fig. 7. Terrain height of DEM used in d03 (shown in Fig. 6) in the reproduced experiment
The large and small rectangles indicate areas mentioned in the results. The dashed line represents vertical section shown in Fig. 16, where both ends A and B correspond to Fig. 16; gray circle indicates location of Rumoi.

datasets are shown in Fig. 7, and areas mentioned in the results are shown using two rectangles.

3. Selection of schemes

WRF offers multiple physics options that can be combined in many ways. Steinhoff et al. (2013) described several physical parameterization schemes of WRF in a case study of a representative summer foehn event over the McMurdo Dry Valleys in Antarctica. Surface states in Hokkaido are similar to those described in that case, and as such, the same schemes can be adopted in the present study. Therefore, for microphysics, the WRF Single-Moment 6-class (WSM6) scheme was used (Hong and Lim, 2006). However, according to Skamarock et al. (2008), several graupel-related terms of this scheme follow those of Lin et al. (1983), but the ice-phase behavior of the scheme is considerably different, owing to the changes made by Hong et al. (2004). However, Dudhia et al. (2008) implemented a procedure unifying the snow and graupel particles by assigning a single fall speed to both that is weighted by the mixing ratios, and this scheme therefore incorporates ice, snow, and graupel processes suitable for high-resolution experiments and is thus used in our study. In addition, the Rapid Radiative Transfer Model (RRTM) scheme was used for long-wave radiation (Mlawer et al., 1997). The molecular species treated in the model are water vapor, carbon dioxide, ozone, methane, nitrous oxide, and the common halocarbons. For short-wave radiation, the Dudhia scheme was used (Dudhia, 1989). Furthermore, the Mellor-Yamada-Nakanishi-Niino (MYNN) scheme was used for the surface layer (Nakanishi, 2001; Nakanishi and Niino, 2004, 2006), and for simulation of the land surface, the Noah Land Surface Model (LSM) with soil temperature and moisture in four layers, fractional snow cover, and frozen soil physics was used (Chen and Dudhia, 2001). The planetary boundary layer was represented by the MYNN level 2.5 (Nakanishi and Niino, 2006), and the cumulus parameterization was that of the Grell-Devenyi (GD) ensemble scheme (Grell and Dévényi, 2002).

IV. Result of numerical experiments

1. Wind distribution at 03:00 LST on January 28, 2003

Figure 8 shows the reproduced experimental results obtained using the WRF model in the study area. A strong wind of approximately 25 m/s is apparent to the south of Mashike, and a wind speed peak also occurs in the vicinity of Rumoi, reaching approximately 18 m/s. The strong wind area near Rumoi spreads out to the Sea of Japan and forms a strong wind area over the sea. However, Mashike itself is associated with a weak wind, and is located between areas of strong winds. In addition, as seen in the northern part of Fig. 8, the coast of the Sea of Japan near Haboro is associated with a relatively weak wind. Therefore, it can be concluded that a strong local wind occurs in the area of Rumoi.

Figure 9 shows the wind speed change at Rumoi, Mashike, and Haboro observed by AMeDAS, and in the numerical experiment from 21:00 LST on January 27, 2003 to 09:00 LST on January 28, 2003. In the observation result represented by the solid lines in Fig. 9, all three points experienced a weak wind of approximately 4 m/s or less at 21:00 LST on January 27, 2003. However, the wind speed at Rumoi subsequently increased, although there was little change in the wind speed at Mashike and Haboro. This again shows that a strong local wind was blowing in Rumoi. According to the numerical experiment result represented by dashed lines in Fig. 9, the numerical experiment tends to overestimate the wind speed especially in Mashike in comparison to the observation, but the overall trend during this event is well-represented, as is the local wind in Rumoi. The wind directions for Rumoi and Mashike are SE and E, respectively. In the southeastern part of Fig. 8, the wind

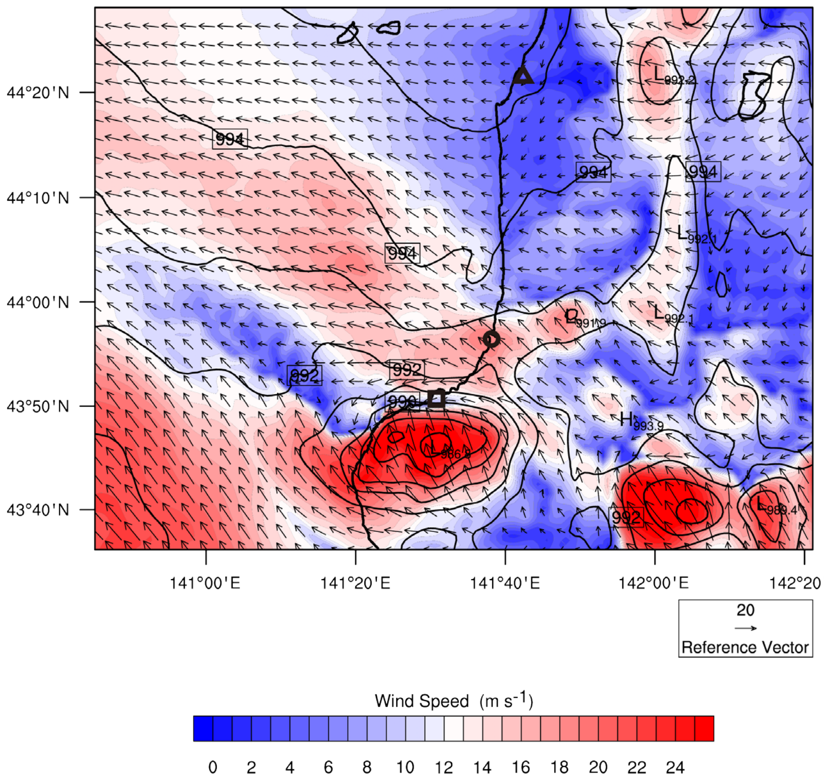

Fig. 8. Numerical experiment result at 03:00 LST on January 28, 2003
Wind vectors represent wind speed and direction, and bold and fine lines represent coastline and isobaric lines of 1 hPa, respectively. In addition, the shading in the figure indicates the scalar values of wind speed at intervals of 1 m/s. The black circle, square, and triangle indicate location of Rumoi, Mashike, and Haboro, respectively.

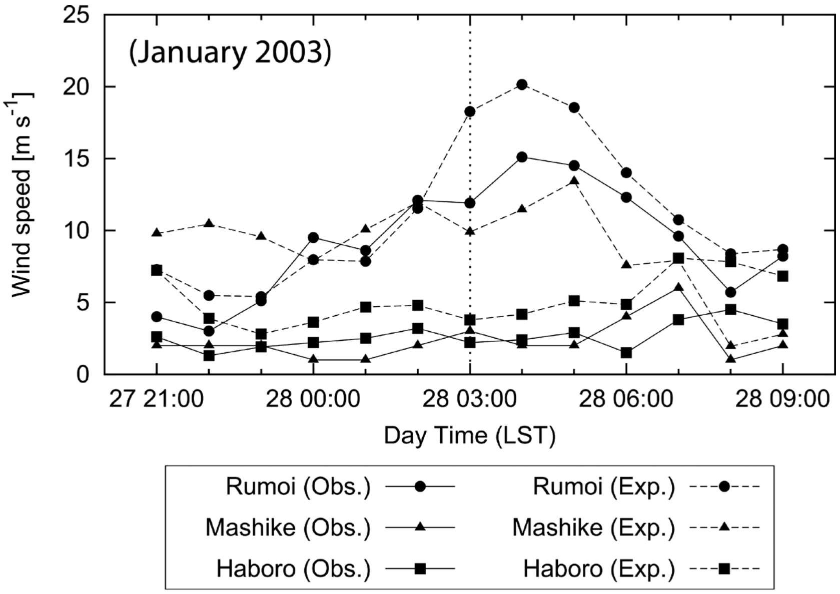

Fig. 9. Temporal variation of observed and simulated wind speed from 21:00 LST on January 27, 2003 to 09:00 LST January 28, 2003
The dotted vertical line in the center shows the time simulated in the present study.

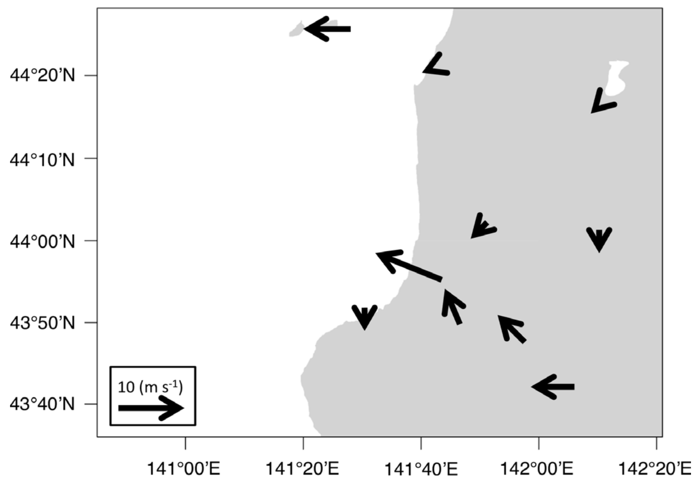

Fig. 10. Wind speed field (03:00 LST on January 28, 2003) observed by AMeDAS around Rumoi

blows towards Rumoi from this direction. Conversely, in the northeastern part of the figure, the wind blows from E to NE, and there is an apparent change in the wind direction.

The result observed by AMeDAS is shown in Fig. 10. Rumoi is determined as being the windiest of all the AMeDAS observation points. The result also shows that there is a strong local wind in Rumoi, in contrast to the weak winds observed in Mashike and Haboro (which agrees with the experimental result). Weak winds are also apparent across both coastal and inland areas. With respect to the wind direction, there was also good correspondence between the numerical experiments and the observations, except near Mashike, where the observations indicate a weak northerly wind but the experiment suggests an easterly wind.

2. Details of events occurring in Rumoi and Mashike at 03:00 LST on January 28, 2003

The previous section clarified the wind conditions in the study area. Figure 11 is a magnified figure using the same data as that presented in Fig. 8, showing the areas around Rumoi and Mashike, but excluding Haboro. A low pressure is located in the south side of Mashike, and wind exists in both the west and east of this area. Additionally, there is a wind stream over the area moving from SE to NW. Mashike is located on the convergence line between two strong wind areas, indicating that the area is experiencing a weak wind. There is also a weak wind area over the Sea of Japan to the west of Mashike, where SE and E winds appear to converge.

3. Wind distribution at 15:00 LST on March 8, 2005

Figure 12 shows the results of another numerical

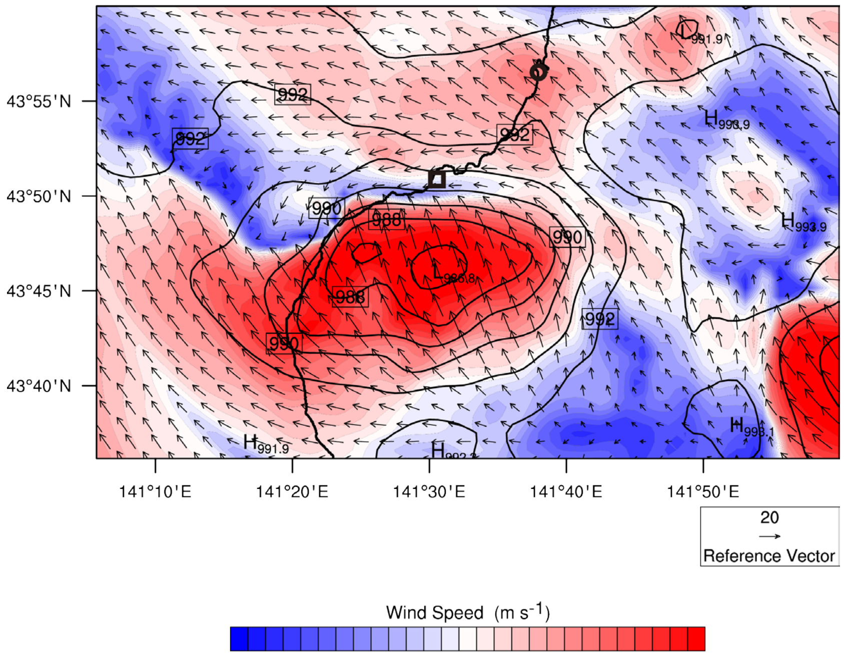

Fig. 11. Same as Fig. 8 (magnified view), but density of wind vectors is different

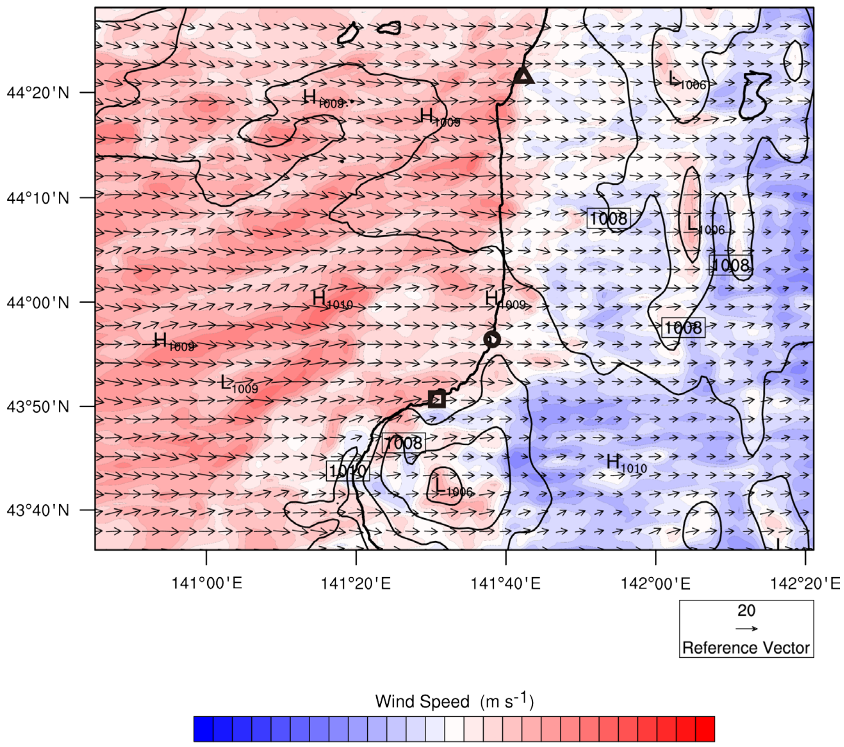

Fig. 12. Same as Fig. 8, but for 15:00 LST on March 8, 2005

experiment obtained using the WRF model in relation to the study area at 15:00 LST on March 8, 2005. The wind speed at sea is approximately 17 m/s, but when the westerly wind reaches the shore, the wind speed weakens and the speed on land is approximately 10 m/s. There is a strong wind blowing along the shore at this time in Rumoi, and the wind speed at Mashike and Haboro is also strong in this respect. According to the wind direction, the prevailing direction is westerly in this area, and this is in good agreement with the pressure gradient from the pressure distribution chart by MANAL (Fig. 5b). There is no local wind direction change at this time, and therefore an evident converging line does not exist. The event is a typical representation of a strong westerly wind blowing from the sea.

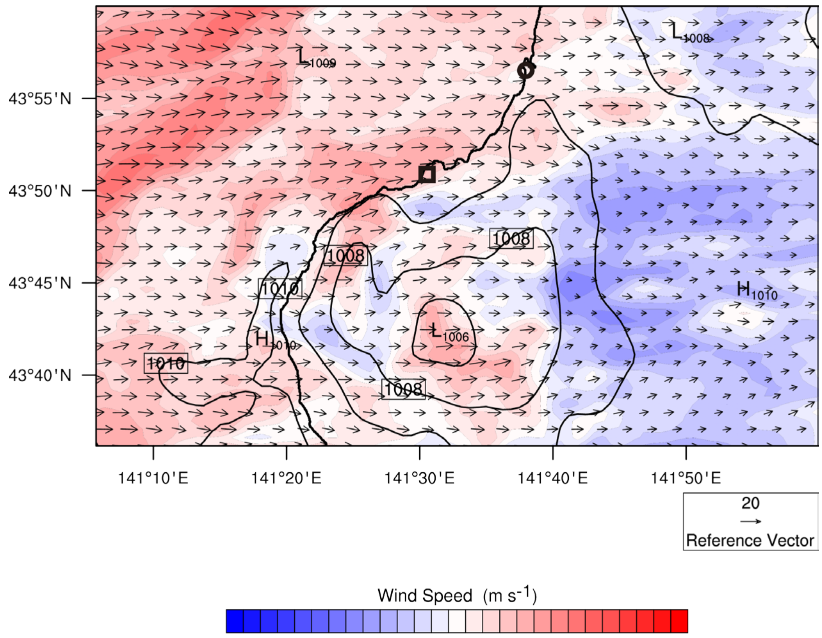

Fig. 13. Same as Fig. 12 (magnified view), but density of wind vectors is different from that in Fig. 12

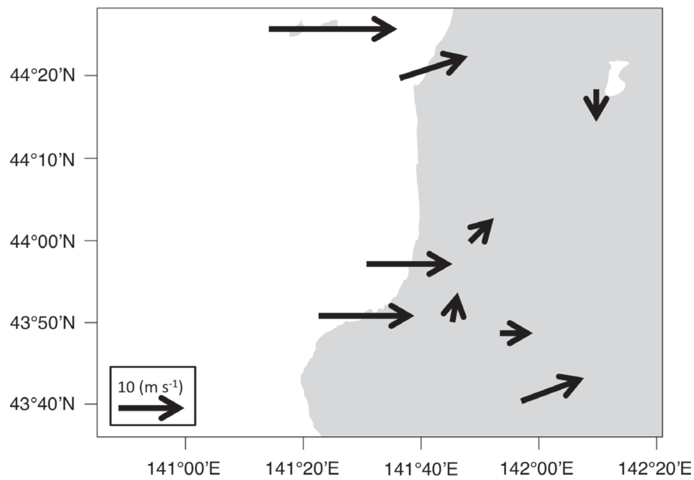

Fig. 14. Same as Fig. 10, but for 15:00 LST on March 8, 2005

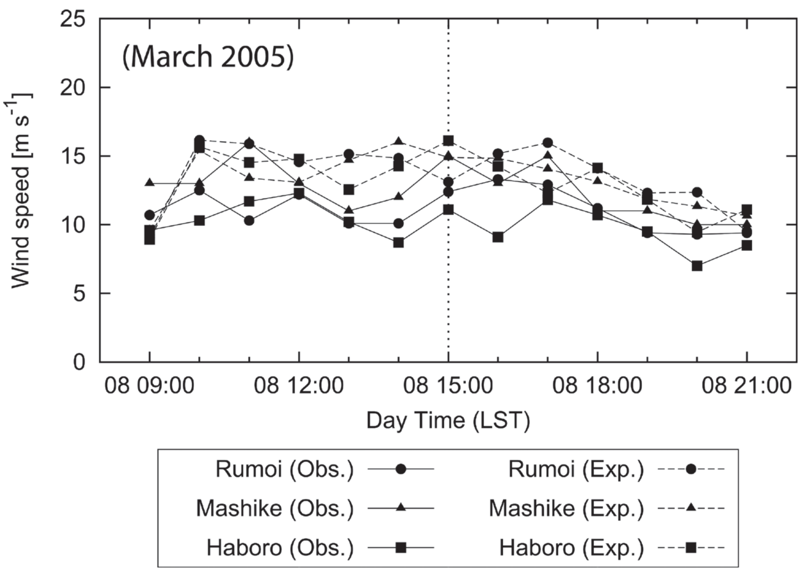

Fig. 15. Same as Fig. 9, but from 09:00 LST to 21:00 LST on March 8, 2005

Figure 13 is a magnified figure adopting the same data as that presented in Fig. 12, where a weak low pressure occurs in the south side of Mashike, but the wind is not separated in this area. There is no convergence line, even on close inspection, and therefore, the wind in Rumoi is as strong as that in Mashike.

Wind speed fields are shown in Fig. 14. Areas where the observed wind speed is relatively high (Rumoi, Mashike, Haboro, Fukagawa, and Yagishiri) are well reproduced, both in relation to wind speed and direction. However, the wind direction in relation to the inland area (Horonuka, Tappu, and Shumarinai) is different from the results of the numerical experiment; the experiment was unable to reproduce the weak northerly and southerly winds.

Figure 15 shows the temporal variation between Rumoi, Mashike, and Haboro. A strong wind was blowing around Rumoi at that time, and this tendency is shown in the result of numerical experiment. However, there was a tendency for the value of the wind speed to be validated highly in the numerical experiments, which is the same tendency as for the previous event.

V. Discussion

1. Consideration of orographic wind

In the previous section, the reproduced experimental result demonstrated the wind distribution for a single point in time. In this section, we describe the temporal variation of the wind speed (shown in Fig. 9) in relation to Rumoi, Mashike, and Haboro, using both observations and numerical experiment for the event in 2003. In Rumoi, the strongest wind measured is approximately 20 m/s; but the maximum wind speeds in Mashike and Haboro are approximately 10 m/s and 5 m/s, respectively. From the start time of the experiment, the wind speed only increased locally in Rumoi, and the wind velocity was seen to be slightly elevated compared to the observation result. According to Fig. 8 and Fig. 10, the wind direction in Mashike is not adequately reproduced for either wind speed or direction. This is because Mashike is located on the convergence line of wind directions, and the resolution of the numerical experiment was not appropriate in this respect. The estimated wind speeds in numerical experiments are systematically larger than those in actual AMeDAS observations. Gómez-Navarro et al. (2015) obtained qualitatively consistent results for complex terrain in the Alps region. They determined that the reproducibility of the ground surface roughness increases and the average distance between the observation point and the nearest grid point is shortened when the spatial resolution is improved, thereby improving the reproducibility of the wind speed.

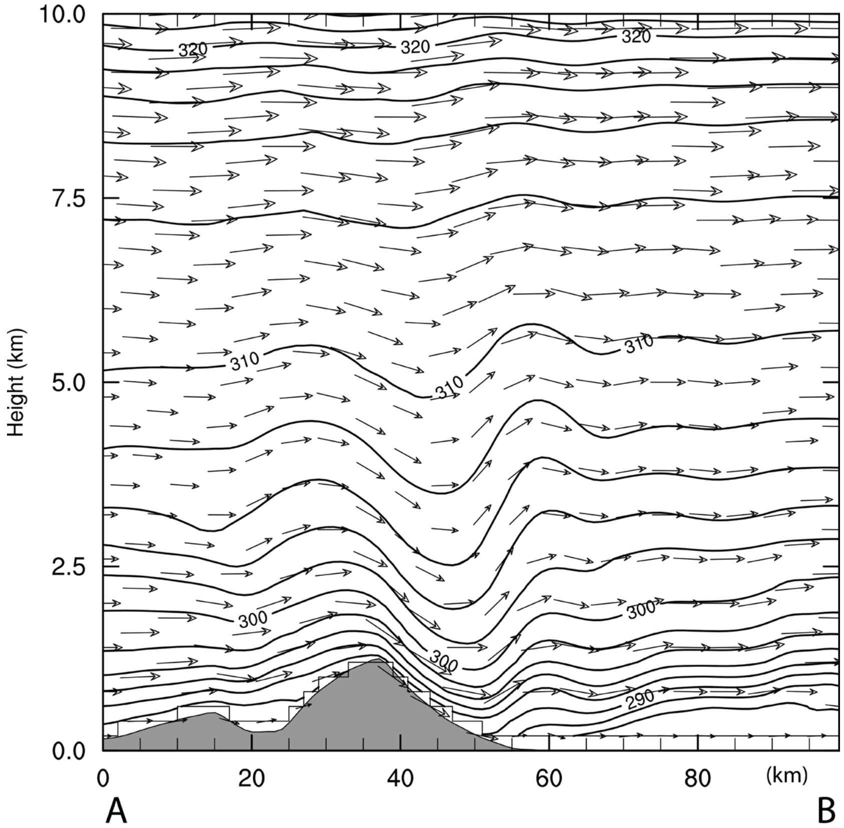

Fig. 16. Vertical distribution chart of wind with DEM height in km
Contour lines show equivalent potential temperature in K. Wind vectors represent V and emphasized W component of wind. Both ends A and B on horizontal axis correspond to those shown in Fig. 7.

However, in this study, the spatial resolution of numerical experiments is high at 1 km, and thus the cause of the systematic overestimation is believed to be the influence of the planetary boundary layer scheme. Unresolved orography is not considered in the MYNN level 2.5 scheme selected in this research; therefore, even at a spatial resolution of 1 km it may be insufficient to express the complex terrain of this research area. As an example of finer experiments, Sheridan and Vosper (2012) carried out numerical simulations with 333-m resolution and reproduced counterflowing wind over the Owens Valley in the Sierra Nevada of California.

The topography of the region may explain why a strong local wind is observed in Rumoi. A lone mountain exists south of Mashike (Mt. Shokambetsu) that reaches a height of 1492 m above sea level (see Fig. 1). From Fig. 11, it is clear that the prevailing wind around this area is forced to change direction near this mountain. In addition, the wind passes through the valley-shaped topography between Fukagawa and Rumoi (see Fig. 1 and Fig. 7), and wind speeds are accelerated in the vicinity of Rumoi. This suggests the existence of a gap wind (e.g., Lackmann and Overland, 1989). A similar result was shown in a study of a local easterly wind “Kiyokawa-dashi” in Japan (Sasaki et al., 2010). To consider the influence of the lone mountain, a cross-sectional view is shown in Fig. 16. The cross section dissects the summit of Mt. Shokambetsu, as indicated by the dashed line in Fig. 7. According to Fig. 16, there is a part of the vertical wind component that is strong, as evidenced by the waving flow of the wind in both upward and downward directions. The distribution of the equivalent potential temperature also varies along the direction of flow, suggesting the presence of a mountain wave extending to a height of approximately 10 km, which is in good agreement with the findings of Ágústsson and Ólafsson (2014).

Kawamura (1963) determined the prevailing wind direction based on wind observation data in Hokkaido, and revealed the distribution of the surface wind direction in winter. Kato (1983) conducted principal component analysis based on the daily average wind speed and atmospheric pressure data in Hokkaido, and created airflow charts. In these previous studies, it is shown that the wind blows from ESE and W in Rumoi, but no mention is made of the strong local wind in Rumoi and its mechanism. In this study, AMeDAS observation data are updated from 1981 to 2010, and strong winds in Rumoi are firstly shown using an analysis of wind speed and direction from data obtained in northwestern Hokkaido. The result of the prevailing wind direction is consistent with that in previous studies, and the mean wind speed of Rumoi is 77% and 33% larger than that in Mashike and Haboro, respectively. In addition, by conducting numerical experiments for the study area or northwestern Hokkaido, it is shown that the strong local wind blows due to the influence of the orography around Rumoi.

2. Sensitivity experiment using surface layer scheme

Finally, a sensitivity experiment was performed to confirm any change in relation to using particular schemes in the numerical experiments. In Hokkaido, the land surface is covered with snow in winter, and therefore, the land

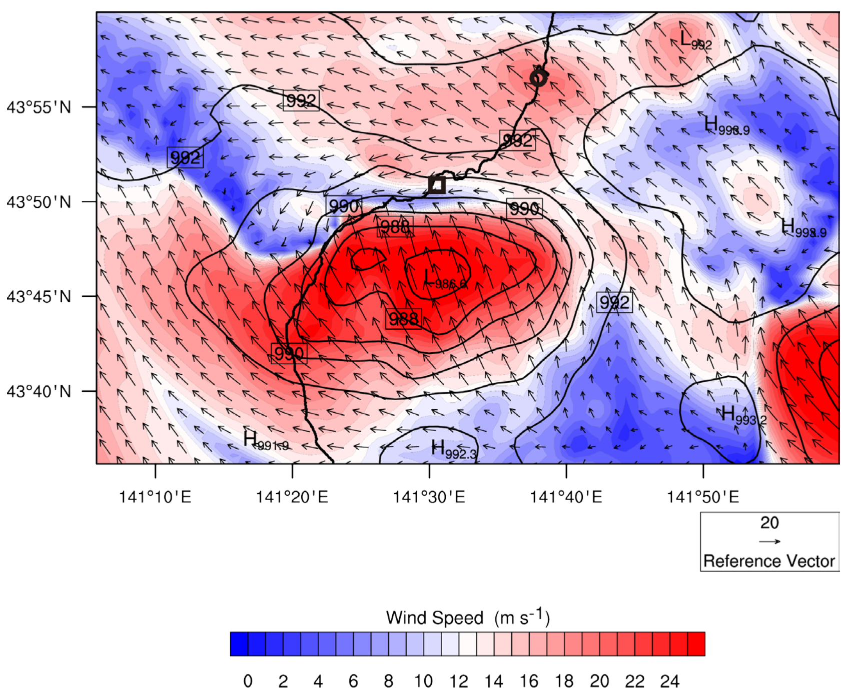

Fig. 17. Sensitivity experiment result (03:00 LST on January 28, 2003)
Wind vectors represent the wind speed and direction, and bold and fine lines represent the coastline and isobaric lines of 1 hPa, respectively. In addition, the shading in the figure indicates the scalar values of wind speed at intervals of 1 m/s. Gray circle indicates the location of Rumoi.

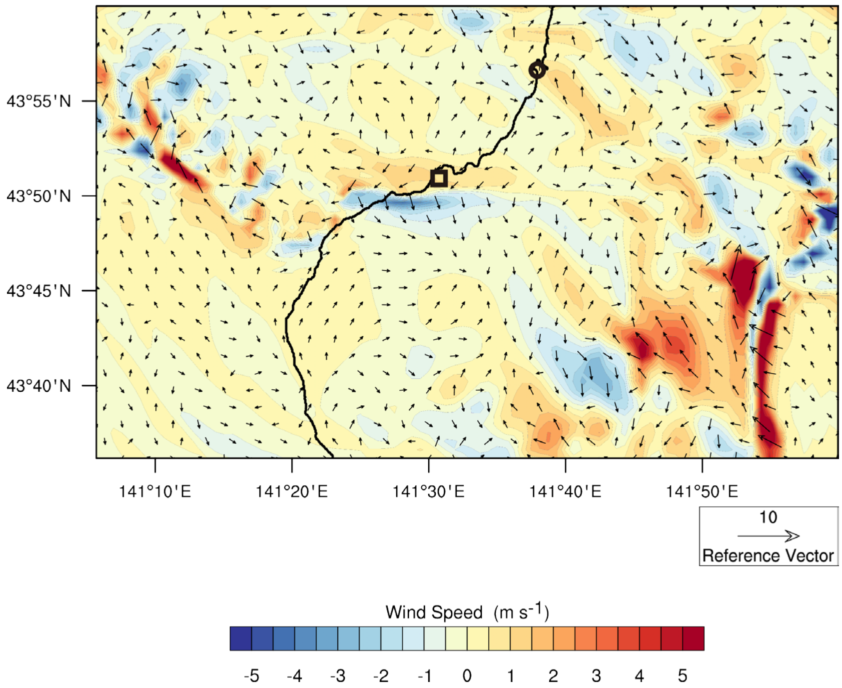

Fig. 18. Difference between sensitivity experiment and numerical experiment (control run)
Shading in figure indicates difference in scalar values of wind speed, and vectors represent vector differences of horizontal wind speed; black circle and square indicate locations of Rumoi and Mashike, respectively.

surface schemes used in the reproduced simulation (Noah LSM) include a simple snow and sea-ice model (Chen and Dudhia, 2001). For the sensitivity experiment, the land surface schemes were, therefore, altered to 5-layer thermal diffusion from the Noah LSM, and the layers are 1, 2, 4, 8, and 16 cm; below these layers, the temperature is fixed at a deep-layer average (Skamarock et al., 2008). However, there are no vegetation processes or snow schemes in the 5-layer thermal diffusion scheme.

The result of the sensitivity experiment is shown in Fig. 17 (magnified view). A comparison between Fig. 17 and Fig. 11 shows that there are no significant differences in the wind directions. With respect to wind speed, a strong local wind at Rumoi and a weak wind area around Mashike, related to the convergence line of the wind, are also reproduced. However, the wind speed is decreased to approximately 2 m/s over the land area. The differences between results using a sensitivity experiment and the numerical experiment (control run) are shown in Fig. 18, which shows an expansion of the strong wind region around Fukagawa and a weaker wind speed near Mashike. The wind speed changes greatly around the convergence line of the wind on the leeward side of Mt. Shokambetsu. The difference in wind vectors shows complex changes, and it appears that this wind change is affected by mountain waves.

Land surface schemes affect ground roughness. Areas covered with snow are relatively smooth, enabling a higher wind speed. The result of the sensitivity experiment can be applied to the discussion of seasonal changes in wind speed at the same pressure distribution condition, but information relating to the physical snow depth is included in the initial data, and this may affect a slight change in the wind in this experiment. The statistical analysis in this study clarified seasonal changes in wind direction at some observation points around Rumoi. Other numerical experiments need to be applied to understand the wind spatial distribution in summer and to discuss seasonal changes of wind.

VI. Conclusions

In this study, a statistical analysis using 30-year AMeDAS datasets of wind speed and direction was performed. The mean wind speed at coastal locations (Rumoi, Mashike, and Haboro) was higher than those in other areas except Fukagawa. The mean wind speed in Rumoi was approximately 5.0 m/s, and the wind speed in Rumoi is relatively strong compared to other locations in northwestern Hokkaido. With respect to a wind frequency analysis, Rumoi had the least frequency (7%) of weak winds (< 5 m/s), and Rumoi recorded the largest number of days with a maximum wind speed of more than 10 m/s as well as the Yagishiri island. As for the wind direction, ESE wind prevails in Rumoi throughout the year, but in winter, the westerly wind occupies more than 30% of the wind. The prevailing wind direction of other points around Rumoi was also ascertained, in addition to its seasonal changes. It was also found that the wind tended to blow from the north in winter at several observation points, in contrast to the direction during summer.

Two numerical experiments using the WRF model were applied to northwestern Hokkaido around Rumoi in order to reproduce the observed weather conditions. One was related to a strong wind event in Rumoi and a weak-wind event occurring concurrently in Mashike and Haboro. The other event related to a simultaneous strong-wind event in Rumoi, Mashike, and Haboro. The results showed that there were good correspondences between the numerical experiments and observations. The numerical experiment results showed that there was a strong wind in Rumoi when the prevailing wind direction was ESE, but Mashike and Haboro experienced weak winds, even when a strong wind blew in Rumoi. This demonstrates that the strong wind over Rumoi is localized. The driving mechanism behind this strong wind is likely to be the result of a gap wind caused by the valley-shaped topography between Fukagawa and Rumoi. Additionally, Mt. Shokambetsu is located to the south of Mashike, and this generates mountain waves that affect the weak local wind over Mashike. However, when the prevailing wind direction is a westerly, the observed wind speeds in Rumoi, Mashike, and Haboro are almost equal, because the strong sea wind reaches these points simultaneously.

A sensitivity experiment was performed to clarify changes in the land surface model of the meteorological model. Results showed that by changing the land surface model to one that did not incorporate snow, there was an alteration in the wind speed over land.

Acknowledgement

We acknowledge Associate Prof. Tomonori Sato for his helpful suggestions, particularly regarding the vertical structure of the wind. We also thank members of the Intelligent Robots and Systems Laboratory, at the Graduate School of Information and Science, Hokkaido University, for discussions in the early stages of this work. This work was supported by JSPS KAKENHI Grant Number JP16J02111.

References

Ágústsson, H. and Ólafsson, H. (2014): Simulations of observed lee waves and rotor turbulence. *Mon. Wea. Rev.*, 142, 832–849.

Akimoto, Y. and Kusaka, H. (2010): Sensitivity of the WRF regional meteorological model to input datasets and surface parameters for the Kanto plain on fine summer days. *Geogr. Rev. Japan*, 83A, 324–340 (in Japanese with English abstract).

Belušić, D., Hrastinski, M., Večenaj, Ž. and Grisogono, B. (2013): Wind regimes associated with a mountain gap at the northeastern Adriatic coast. *J. Appl. Meteor. Climatol.*, 52, 2089–2105.

Chen, F. and Dudhia, J. (2001): Coupling an advanced land surface-hydrology model with the Penn state-NCAR MM5 modeling system. Part I: Model implementation and sensitivity. *Mon. Wea. Rev.*, 129, 569–585.

Defant, F. (1951): *Compendium of Meteorology*, chap. Local winds, 655–672, Amer. Meteor. Soc.

Dudhia, J. (1989): Numerical study of convection observed during the winter monsoon experiment using a mesoscale two-dimensional model. *J. Atmos. Sci.*, 46(20), 3077–3107.

Dudhia, J., Hong, S-Y. and Lim, K-S. (2008): A new method for representing mixed-phase particle fall speeds in bulk microphysics parameterizations. *J. Meteor. Soc. Japan*, 86A, 33–44.

Gómez-Navarro, J.J., Raible, C.C. and Dierer, S. (2015): Sensitivity of the WRF model to PBL parametrisations and nesting techniques: evaluation of wind storms over complex terrain. *Geosci. Model Dev.*, 8, 3349–3363.

Grell, G.A., Dudhia, J. and Stauffer, D.R. (1994): A Description of the fifth-generation Penn State/NCAR Mesoscale Model (MM5). *NCAR Technical Note*, 121 pp.

Grell, G.A. and Dévényi, D. (2002): A generalized approach to parameterizing convection combining ensemble and data assimilation techniques. *Geophys. Res. Lett.*, 29(14), doi:10.1029/2002GL015311, 2002.

Hong, S-Y. and Lim, J.-O.J. (2006): The WRF single-moment 6-class microphysics scheme (WSM6). *J. Korean Meteor. Soc.*, 42, 129–151.

Hong, S-Y., Dudhia, J. and Chen, S-H. (2004): A revised approach to ice microphysical processes for the bulk parameterization of clouds and precipitation. *Mon. Wea. Rev.*, 132, 103–120.

Horvath, K., Koracin, D., Vellore, R., Jiang, J. and Belu, R. (2012): Sub-kilometer dynamical downscaling of near-surface winds in complex terrain using WRF and MM5 mesoscale models. *J. Geophys. Res.*, 117, D11111, doi:10.1029/2012JD017432.

Inamura, T., Iwasaki, K., Saito, H., Nakayama, D., Izumi, T. and Matsuyama, H. (2009): Numerical simulation investigating how local wind “Matsubori-Kaze” is affected by unique topography of Mt. Aso. *Tenki*, 56, 123–138 (in Japanese).

Jiménez, P.A. and Dudhia, J. (2013): On the ability of the WRF model to reproduce the surface wind direction over complex terrain. *J. Appl. Meteor. Climatol.*, 52, 1610–1617.

Kasai, K. and Kimura, K. (2013): Climate change analysis of Hokkaido by mesh data using Koeppen climate classification. *Geographical Studies*, 88, 37–48 (in Japanese with English abstract).

Kato, H. (1983): Regionality of surface wind in Hokkaido – an analysis by means of PCA –, *Environmental Science, Hokkaido University*, 5, 293–304 (in Japanese).

Kawaguchi, J., Kusaka, H. and Kimura, F. (2010): Analyses of southerly winds along the Kitakami basin when the

Yamase prevails. *Geogr. Rev. Japan*, 83A, 375–383 (in Japanese with English abstract).

Kawai, T., Nakajyo, M., Kato, H. and Yamakawa, S. (2008): Climatological characteristics of local wind in the Tokachi district, Hokkaido, Japan. *Proceedings of the Institute of Natural Sciences, Nihon University*, 43, 287–302 (in Japanese).

Kawamura, T. (1963): Surface wind distribution in Hokkaido in winter. *J. Meteor. Res.*, 15, 533–537 (in Japanese).

Kawamura, T. (1966): Surface wind systems over central Japan in the winter season – with special reference to winter monsoons –, *Geogr. Rev. Japan*, 39, 538–554 (in Japanese with English abstract).

Kawamura, T. (1981): Area wind systems over Japan. *Journal of Architecture and Building Science*, 96(1185), 39–42 (in Japanese).

Kusaka, H. (2009): About a regional atmospheric model, WRF. *Nagare*, 28, 3–12 (in Japanese).

Lackmann, G.M. and Overland, J.E. (1989): Atmospheric structure and momentum balance during a gap-wind event in Shelikof Strait, Alaska. *Mon. Wea. Rev.*, 117, 1817–1833.

Lin, Y-L., Farley, R.D. and Orville, H.D. (1983): Bulk parameterization of the snow field in a cloud model. *J. Climate Appl. Meteor.*, 22, 1065–1092.

Mlawer, E.J., Taubman, S.J., Brown, P.D., Iacono, M.J. and Clough, S.A. (1997): Radiative transfer for inhomogeneous atmospheres: RRTM, a validated correlated-k model for the longwave. *J. Geophys. Res.*, 102D, 16663–16682.

Nakanishi, M. (2001): Improvement of the Mellor-Yamada turbulence closure model based on large-eddy simulation data. *Boundary-Layer Meteorol.*, 99, 349–378.

Nakanishi, M. and Niino, H. (2004): An improved Mellor-Yamada level-3 model with condensation physics: its design and verification. *Boundary-Layer Meteorol.*, 112, 1–31.

Nakanishi, M. and Niino, H. (2006): An improved Mellor-Yamada level-3 model: its numerical stability and application to a regional prediction of advection fog. *Boundary-Layer Meteorol.*, 119, 397–407.

National Centers for Environmental Prediction/National Weather Service/NOAA/U.S. Department of Commerce (2000): *NCEP FNL Operational Model Global Tropospheric Analyses, continuing from July 1999*. Research Data Archive at the National Center for Atmospheric Research, Computational and Information Systems Laboratory. https://doi.org/10.5065/D6M043C6. Accessed 12 Feb 2017.

Powers, J.G. (2007): Numerical prediction of an Antarctic severe wind event with the weather research and forecasting (WRF) model. *Mon. Wea. Rev.*, 135, 3134–3157.

Prtenjak, M.T., Viher, M. and Jurković, J. (2010): Sea-land breeze development during a summer bora event along the north-eastern Adriatic coast. *Quart. J. Roy. Meteor. Soc.*, 136, 1554–1571.

Reynolds, R.W., Smith, T.M., Liu, C., Chelton, D.B., Casey, K.S. and Schlax, M.G. (2007): Daily high-resolution-blended analyses for sea surface temperature. *J. Climate*, 20, 5473–5496.

Sagawa, M. (2004): Features of wind speed and direction over a strong wind area in Suttsu district, Hokkaido, Japan. *Geogr. Rev. Japan*, 77, 441–459 (in Japanese with English abstract).

Sakamoto, M., Inamura, T., Izumi, T. and Matsuyama, H. (2014): An observational study on the blowing extent and mechanism of “Matsubori-kaze” based on in situ observations and meso-scale meteorological model. *Tenki*, 61, 977–996 (in Japanese).

Sasaki, K., Sawada, M., Ishii, S., Kanno, H., Mizutani, K., Aoki, T., Itabe, T., Matsushima, D., Sha, W., Noda, A.T., Ujiie, M., Matsuura, Y. and Iwasaki, T. (2010): The temporal evolution and spatial structure of the local easterly wind “Kiyokawa-dashi” in Japan Part II: Numerical simulations. *J. Meteor. Soc. Japan*, 88, 161–181.

Sheridan, P. and Vosper, S. (2012): High-resolution simulations of lee waves and downslope winds over the Sierra Nevada during T-REX IOP 6. *J. Appl. Meteor. Climatol.*, 51, 1333–1352.

Skamarock, W.C. (2004): Evaluating mesoscale NWP models using kinetic energy spectra. *Mon. Wea. Rev.*, 132, 3019–3032.

Skamarock, W.C., Klemp, J.B., Dudhia, J., Gill, D.O., Barker, D.M., Duda, M.G., Huang, X-Y., Wang, W. and Powers, J.G. (2008): A Description of the Advanced Research WRF Version 3. *NCAR Technical Note*, 113 pp.

Steinhoff, D.F., Bromwich, D.H. and Monaghan, A. (2013): Dynamics of the Foehn mechanism in the McMurdo Dry Valleys of Antarctica from polar WRF. *Quart. J. Roy. Meteor. Soc.*, 139, 1615–1631.

Suzuki, R. (1991): The response of the surface wind speed to the synoptic pressure gradient in central Japan. *J. Meteor. Soc. Japan*, 69, 389–399.

Suzuki, R. (1992): The angle of deflection between the mean vector of the surface wind and the geostrophic wind vector over central Japan. *J. Meteor. Soc. Japan*, 70, 703–710.

Suzuki, R. (1994): Surface geostrophic and observed winds in the coastal zone of Japan. *J. Meteor. Soc. Japan*, 72, 81–90.

Takane, Y., Ohashi, Y., Kusaka, H., Shigeta, Y. and Kikegawa, Y. (2013): Effects of synoptic-scale wind under the typical summer pressure pattern on the mesoscale high-temperature events in the Osaka and

Kyoto urban areas by the WRF model. *J. Appl. Meteor. Climatol.*, 52, 1764–1778.

Tatsumi, K., Takemi, T. and Ishikawa. H. (2008): A high-resolution weather simulation system based on the WRF model: A case study for a heavy rainfall. *Annuals of Disas. Prev. Res. Inst., Kyoto University*, 51B, 437–448 (in Japanese).

Weiss, S.J., Pyle, M.E., Janjic, Z., Bright, D.R., Kain, J.S. and DiMego, G.J. (2008): The operational high resolution window WRF model runs at NCEP: Advantages of multiple model runs for severe convective weather forecasting. Preprints, *24th Conf. on Severe Local Storms, Savannah, GA, Amer. Meteor. Soc.*, P10.8. [Available online at https://ams.confex.com/ams/pdfpapers/142192.pdf]

Zhang, C., Wang, Y., Lauer, A. and Hamilton, K. (2012): Configuration and evaluation of the WRF model for the study of Hawaiian regional climate. *Mon. Wea. Rev.*, 140, 3259–3277.

Zhang, H., Pu, Z. and Zhang, X. (2013): Examination of errors in near-surface temperature and wind from WRF numerical simulations in regions of complex terrain. *Wea. Forecasting*, 28, 893–914.

(Accepted on 17 June 2017)

北海道北部西岸における局地的強風に関する解析

葛西　光希[1]，木村　圭司[2]，塩見　慶[3,4]，近野　敦[4]，田殿　武雄[3,4]，堀　雅裕[3,4]

[1] 北海道大学大学院情報科学研究科・院生
[2] 奈良大学文学部
[3] 宇宙航空研究開発機構地球観測研究センター
[4] 北海道大学大学院情報科学研究科

要旨

北海道北西部に位置する留萌において局地的強風が観測される。留萌周辺における風について調査するために，30 年間の AMeDAS による風の観測結果の解析と Weather Research and Forecasting (WRF) モデルによる数値実験を行った。
解析結果より，留萌は周辺の他の地点と比較して風が強く，かつ頻度に着目した場合においては他の地点よりも強風が吹く頻度が高い。風向の季節変化については，夏季の留萌においては東南東風が半分以上の割合で吹走する一方，冬季の留萌では西風の割合が高くなるということが明らかになった。
冬季の留萌周辺において局地的強風が吹走する原因を明らかにするため，二つの事例について数値実験を行い，比較を行った。一つは留萌において 12 m/s 程度の強風が吹き，かつ周辺地域では 5 m/s 程度の弱風となっている 2003 年 1 月 28 日午前 3 時の事例である。このときの卓越風向は東南東となっていた．他方は，研究対象地域全体にわたって 10 m/s 以上の強風が吹いていた事例である（2005 年 3 月 8 日午後）。このときの卓越風向は西風である．実験結果は観測結果と概ねよい一致を得られ，実験結果から留萌で局地的強風が吹走するときの鉛直断面図を作成することにより，付近に山岳波の存在が示された。また，風が谷状の地形を吹走し，留萌周辺で風が加速されている。このことは，地峡風の存在を示唆している。最後に，地表面のモデルについて雪を考慮しないスキームを設定することにより感度実験を行った。風向にはほとんど変化がないものの，風速が 2 m/s 程度減少するという結果が得られた。

キーワード：局地風，数値実験，統計解析，風速，地形の影響